Journal of Power Sources 247 (2014) 142–150

Contents lists available at ScienceDirect

Journal of Power Sources

journal homepage: www.elsevier.com/locate/jpowsour

PtSn/C catalysts for ethanol oxidation: The effect of stabilizers on the morphology and particle distribution

Yanjiao Ma [a], Hui Wang [a], Shan Ji [b,1], Vladimir Linkov [b], Rongfang Wang [a,*]

[a] Key Laboratory of Eco-Environment-Related Polymer Materials, Ministry of Education of China, College of Chemistry and Chemical Engineering, Northwest Normal University, Lanzhou 730070, China
[b] South African Institute for Advanced Materials Chemistry, University of the Western Cape, Private Bag X17, Bellville 7535, Cape Town, South Africa

HIGHLIGHTS

- PtSn/C catalysts were prepared by the different stabilizers.
- PtSn/C catalysts showed different electrocatalytic activity toward ethanol oxidation.
- PtSn/C glycine catalyst showed the better performance due to nano-structured morphology.

GRAPHICAL ABSTRACT

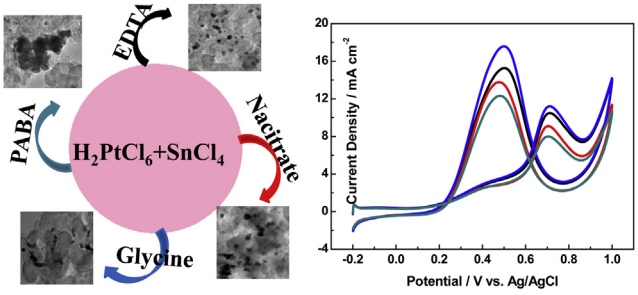

ARTICLE INFO

Article history:
Received 3 July 2013
Received in revised form
17 August 2013
Accepted 20 August 2013
Available online 31 August 2013

Keywords:
Platinum–tin alloy
Different stabilizers
Nanostructure
Electrocatalysts
Ethanol oxidation

ABSTRACT

PtSn/C catalysts are synthesized by using four stabilizers, i.e., ethylene diamine tetra-acetic acid (EDTA), sodium citrate (NaCitrate), glycine and P-aminobenzoate (PABA) with the same reducing process and reaction parameters. XRD characterization shows all PtSn/C catalysts possess face-centered cubic structure with different alloying degree. TEM results show that stabilizers have a significant impact on the morphology and particle size distribution. PtSn/C EDTA and glycine have good particle dispersion with sphere and short nanowire morphology, while obvious particle agglomeration occurred on PtSn/C NaCitrate and PtSn/C PABA. Electrocatalytic activities of these PtSn/C catalysts for ethanol electro-oxidation are also measured by cyclic voltammetry. Enhancement of electrocatalytic activity is ascribed to the high particle distribution of PtSn nanoparticles on the carbon supports, not the alloying degree of PtSn nanoparticles. The difference of glycine activities between PtSn/C EDTA and PtSn/C glycine could be ascribed to the variation in the amount of Sn oxides on the surface and density of inter-grain boundary regions in PtSn nanoparticles.

1. Introduction

PtSn nanoparticles deposited on carbon support were reported as the most effective catalyst for the ethanol oxidation reaction (EOR) among various Pt-based binary catalysts [1]. The electrochemical oxidation of ethanol has been extensively studied on PtSn catalysts with different compositions and structure, which were prepared by a variety of methods, such as carbon co-impregnation followed by reduction [2], Bonneman's method [3], and modified polyol method [4,5]. By analyzing these reports on preparing binary PtSn catalysts [4,6–8], it seems that there has three similar characteristics of PtSn binary catalysts, i) to form Pt_3Sn phase but not exclusive; ii) part of the Sn was not alloyed with Pt but in oxidized

* Corresponding author. Tel./fax: +86 931 7971533.
E-mail addresses: sji@uwc.ac.za (S. Ji), wrf38745779@126.com, wangrf@nwnu.edu.cn (R. Wang).
[1] Tel./fax: +27 21 9599316.

0378-7753/$ – see front matter © 2013 Elsevier B.V. All rights reserved.
http://dx.doi.org/10.1016/j.jpowsour.2013.08.086

state; iii) the excellent EOR activity of PtSn/C catalyst were explained by bifunctional mechanism and electronic effect.

In order to improve activity of PtSn/C catalysts towards EOR, effect of the synthesis methods on the composition and structure which have a huge impact on glycine activity of PtSn/C, has been extensively studied. García-Rodríguez et al. compared PtSn/C catalysts prepared by colloidal and impregnation–reduction methods, respectively; the results suggested PtSn/C catalyst prepared by impregnation–reduction method showed better activity than that by colloidal method [2]. Pt:Sn atomic ratio of 1:3 has been proved as the optimal ratio of PtSn/C catalysts for EOR [1,4,8–11]. Other parameters, such as concentration of reductant [12], pH of solutions [13] and temperature of heat-treatment [14,15], etc., were also investigated by some research groups. These reports on PtSn binary materials show that the electrocatalytic activity of PtSn/C catalyst is strongly dependent on synthesis conditions. The procedure of synthesizing PtSn/C has a major influence on the physical properties of PtSn nanoparticle, such as composition, structure, and degree of alloying, which results in different electrocatalytic activities in EOR.

Recently, Somodi et al. [16] and Wang et al. [17] prepared PtSn bimetallic nanoparticles with different morphology and particle sizes by using different stabilizers. However, electrocatalytic performance of these PtSn nanoparticles is not investigated in these reports. In the work of Liu et al. [18], the catalytic activity of the Pt_3Sn nanoparticles for methanol oxidation were studied and found that the good disperse results in good catalytic activity. Unfortunately, as the most efficient catalyst for ethanol oxidation, the effect of the particle size distribution and morphology of PtSn/C catalyst derived from the different stabilizers on the catalytic activity haven't been investigated. Thus, it will be an interesting work to investigate the effect of stabilizers on the electrocatalytic performance. In this work, various stabilizers were used to synthesize PtSn nanoparticles and EOR was chosen to evaluate the effect of morphology of PtSn nanoparticles on the electrocatalytic performance. It was found that there are considerable differences in electrocatalytic activities toward EOR on these PtSn/C catalysts with different morphology.

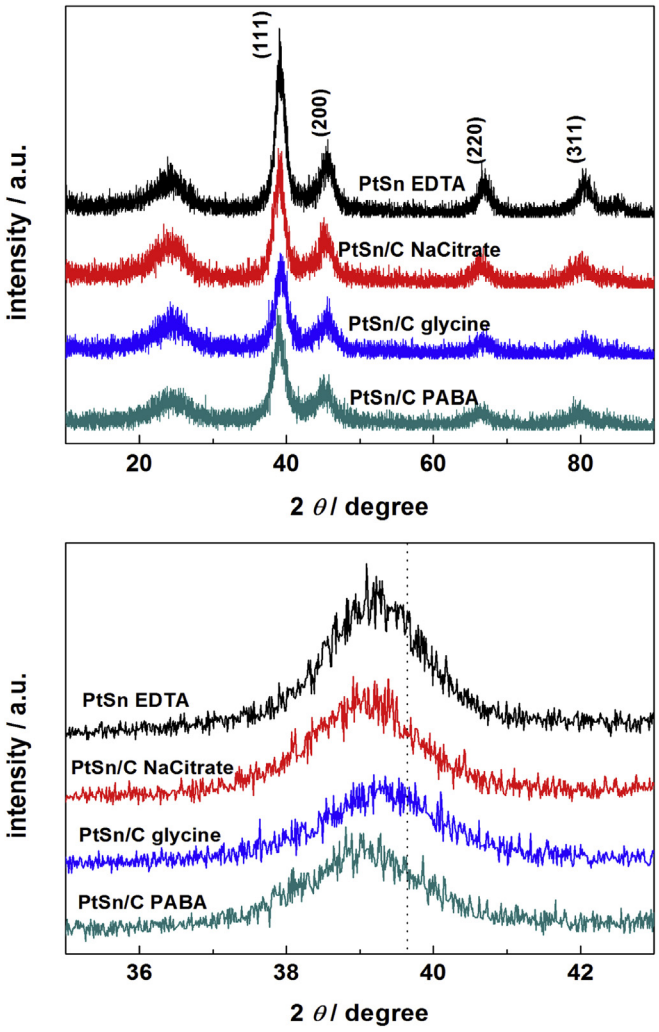

Fig. 1. XRD patterns of PtSn/C catalysts (a) PtSn/C EDTA; (b) PtSn/C NaCitrate; (c) PtSn/C glycine; and (d) PtSn/C PABA.

2. Experimental

2.1. Preparation of PtSn/C catalysts

PtSn/C catalysts were prepared by $NaBH_4$ reduction method, which was carried out in alkaline ethylene glycol (EG) solution. PtSn/C catalysts with Pt:Sn atomic ratio of 3:1 were prepared as follows: 4.12 mL of 20 mg mL^{-1} H_2PtCl_6 aqueous solutions, 18.58 mg of $SnCl_4 \cdot 6H_2O$ were dissolved in 30 mL ethylene glycol (EG) and stirred for 0.5 h. Then the stabilizer, i.e., 260 mg of ethylene diamine tetra-acetic acid (EDTA), was added and kept stirring for 0.5 h. Pretreated carbon black Vulcan® XC-72R (150 mg) was added to the mixture with stirring. pH value of the mixture was adjusted to ~10 by using 5 wt% KOH/EG solution with vigorous stirring. After that, 40 mL of 0.2 mol L^{-1} $NaBH_4$ aqueous solution was added slowly to the mixture and kept stirring for 12 h. The resultant, PtSn/C EDTA, was collected by filtrating, washed with deionized water 5 times and dried in air at 60 °C for 12 h.

Subsequently, sodium citrate (NaCitrate), glycine and P-aminobenzoate (PABA) were used to prepare PtSn/C catalysts. Taking into account the effect of the concentration of the stabilizers on morphology and disperse of metal particles, the normal molar ratio of the stabilizer and metal ion for EDTA and glycine is ca. 4:1, while that is ca. 1:1 for NaCitrate and PABA. It should be noted that the quantities of these stabilizers are light excess. The procedures were the same as the above one, except 80 mg of NaCitrate, 69 mg of glycine and 60 mg of PABA were added as stabilizer instead of EDTA, respectively.

2.2. Characterization

X-ray diffraction (XRD) patterns of the catalysts were recorded on a Shimadzu XD-3A diffractometer (Japan) using filtered Cu Kα radiation. Transmission electron microscopy (TEM) measurement was carried out on a JEM-2010 Electron Microscope (Japan) with the acceleration voltage of 200 kV. The average chemical compositions of the catalysts were determined using an IRIS advantage inductively coupled plasma atomic emission spectroscopy (ICP-AES) system (Thermo, USA) with the energy dispersive X-ray analysis (EDX) technique coupled to the TEM.

2.3. Electrochemical measurements

Electrochemical analysis were carried out on a CHI650D electrochemical work station. A conventional three-electrode electrochemical cell was used, comprising a platinum counter electrode and an Ag/AgCl (3 mol L^{-1} KCl) reference electrode. The working electrode was prepared using 5 mg of catalyst dispersed ultrasonically in 1 mL of Nafion/ethanol solution (0.25 wt% Nafion), then 8 μL of the dispersion was transferred onto a glassy carbon (GC) disc

Table 1
Structural parameters and alloying degree of the PtSn/C EDTA, PtSn/C NaCitrate, PtSn/C glycine and PtSn/C PABA catalysts.

Catalyst	PtSn/C EDTA	PtSn/C NaCitrate	PtSn/C glycine	PtSn/C PABA
The mean crystallite size/nm	7.4	6.4	6.1	6.2
Lattice constant/Å	3.980	3.996	3.978	3.999
The content of alloyed Sn/%	17.5	23.4	16.8	24.6
The loading of metal/wt%	20.8	19.9	20.2	21.0
Pt:Sn atom ratio	3.05:1	2.98:1	3.01:1	3.15:1
The average particle size/nm	7.4	9.5	7.2	–

(5 mm in diameter) using a pipette and then dried in air. The solution was purged with high-purity N_2 for at least 30 min to ensure gas saturation before each measurement, and stable voltammograms recorded after 10 cycles were taken into account for the all experiments. All electrochemical measurements were carried out at ambient temperature.

3. Results and discussion

XRD patterns were conducted to characterize the crystalline structure and calculate alloying degree of PtSn/C catalysts (Fig. 1). It was found that XRD patterns of these four PtSn/C catalysts made from different stabilizers are quite similar. The peak at around 25° is attributed to the (002) plane of the hexagonal structure of Vulcan XC-72R carbon support [19]. All samples display four diffraction peaks of Pt (111), Pt (200), Pt (220) and Pt (311) at the corresponding diffraction position, indicating that PtSn nanoparticles made from different stabilizers possess the face centered cubic (fcc) platinum on their surface. The diffraction peaks related to tin oxides weren't observed in these XRD patterns, indicating tin oxides may be amorphous.

The enlarged (111) peaks of these PtSn/C catalysts are presented in Fig. 1b. For comparison, the (111) diffraction peak of Pt/C [19] is also plotted as the vertical dotted line in this figure. Compared with Pt/C, left shift of the (111) peak was clearly observed for the four PtSn/C catalysts. This shift, resulting from the increased lattice parameter of the fcc crystal structure of Pt, provides an evidence that Sn atoms were incorporated into Pt cubic lattice [17]. Furthermore, the left shifts of the Pt (111) peaks follow the order: PtSn/C EDTA ≈ PtSn/C glycine < PtSn/C NaCitrate ≈ PtSn/C PABA, implying that stabilizers do have significant influence on the structure of resulted PtSn/C.

The mean crystallite size of PtSn/C catalysts were calculated using Scherrer's formula [20]:

$$d = \frac{\kappa\lambda}{\beta\cos\theta} \quad (1)$$

where θ is the Bragg's diffraction angle for the peak, κ is Scherrer's constant, $\lambda = 0.154$ nm is the X-ray radiation wavelength, and β (unit: radians) is the full-width at half-maximum intensity (FWHM) of the peak. The FWHM of the peak corresponding to

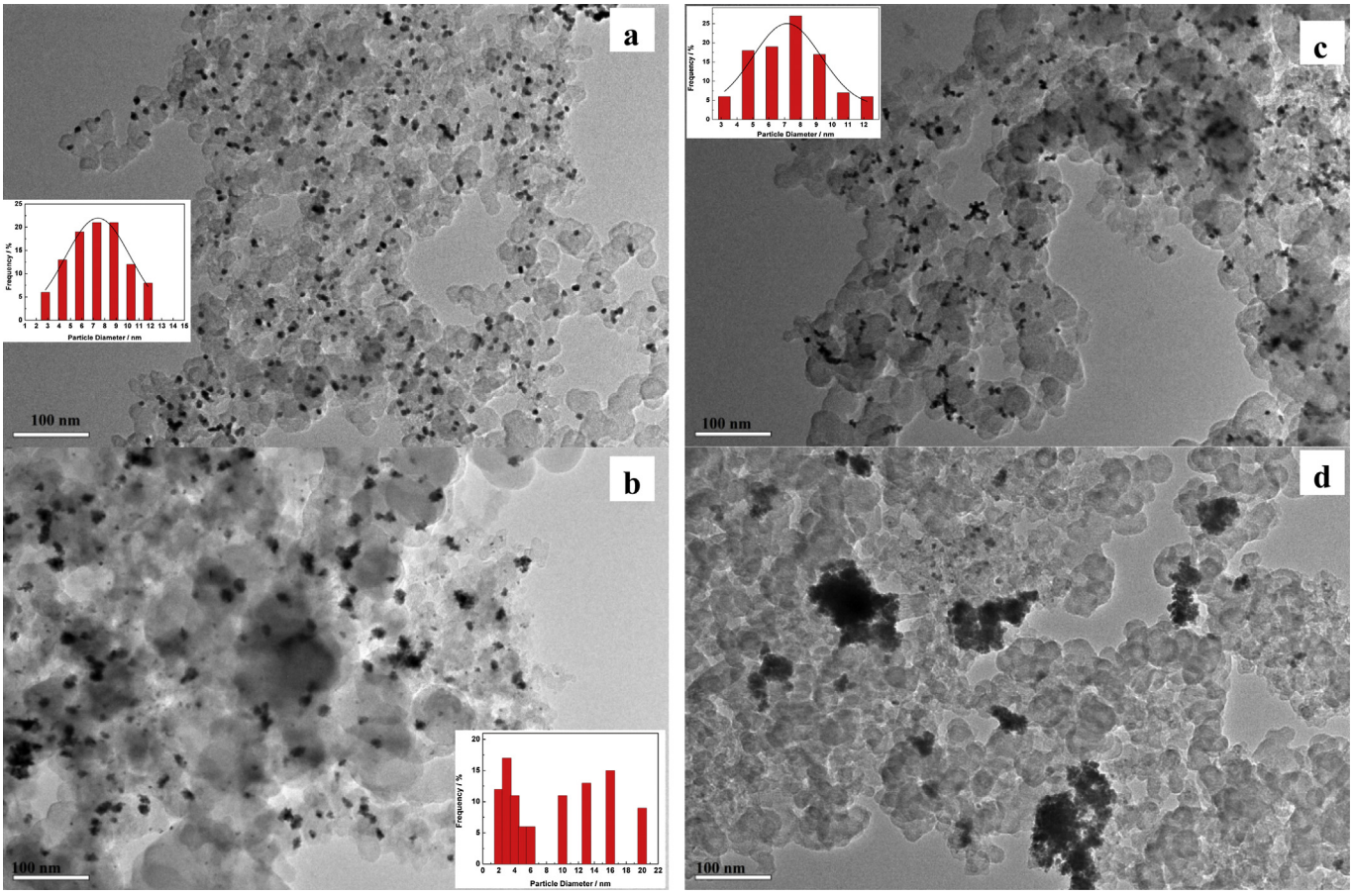

Fig. 2. Representative TEM images and the corresponding particle size distribution histogram of PtSn/C catalysts: (a) PtSn/C EDTA; (b) PtSn/C NaCitrate; (c) PtSn/C glycine; and (d) PtSn/C PABA.

(220) crystal planes of Pt was selected to minimize interference from overlapping peaks of carbon. The calculated average crystallite sizes of PtSn/C are listed in Table 1, which shows that the stabilizers can affect the crystallite size.

The lattice parameters for the four catalysts were calculated according to Equation (2) [21]

$$\alpha(\mathrm{fcc}) = \frac{\sqrt{2}\lambda}{\sin\theta} \tag{2}$$

where $\alpha_{(\mathrm{fcc})}$ is the lattice parameter and λ is the X-ray radiation wavelength. The obtained lattice parameters for the four catalysts are tabulated in Table 1. Following a procedure described in the literature [21], the amount of alloyed Sn (f_{Sn}) in the PtSn catalysts can be calculated using the relationship

$$f_{\mathrm{Sn}} = \left[\frac{\alpha_c - \alpha_0}{\alpha_s - \alpha_0}\right] x_s \tag{3}$$

Where α_c is the experimental lattice parameter, $\alpha_0 = 0.39231$ nm was chosen according to literature [16], α_s is the network parameter for Pt_3Sn/C (0.40015 nm, ca. 100% alloyed), and x_s is the Sn atomic fraction (0.25). The values of calculated f_{Sn} are listed in Table 1. The calculated f_{Sn} values of these catalysts are different, indicating that the different stabilizers used in the same procedure result in formed PtSn with different alloying degrees.

The actual bulk compositions of all PtSn/C catalysts, measured by ICP, are presented in this Table 1. The Pt:Sn atomic ratios were quite close to the Pt:Sn atomic ratio (3:1) in the precursors. The metal loading for each catalyst is similar, and slightly lower than that in the precursors.

Particle size distributions of the PtSn nanoparticles formed on carbon are measured by TEM analysis. Fig. 2 presents the TEM images of PtSn/C synthesized using different stabilizers and their corresponding particle size distribution histogram. For PtSn/C EDTA catalyst (Fig. 2a), the dark spots of PtSn nanoparticles have an ellipse shape with uniform particle size distribution. The average diameter of the PtSn nanoparticles is ca. 7.4 nm, which is in good accordance with the XRD result. In the case of PtSn/C NaCitrate (Fig. 2b), quasi-spherical PtSn nanoparticles were formed with wide particle size distribution. The size of the PtSn nanoparticles ranges from 1.5 nm to 20 nm. The average diameter of the PtSn nanoparticles is ca. 9.5 nm, which is obviously larger than the XRD result due to the agglomeration. XRD gives information on the size of a coherent scattering domain, agglomerates, comprising crystallites with different lattice orientations, which appear in XRD patterns undistinguishable from isolated particles. Thus, the obvious difference of particle size obtained from XRD and TEM is inevitable. The particle agglomeration is often not considered in utilisation of TEM rather than XRD for determining particle dispersion. Fig. 2c shows that particle size distribution of PtSn/C glycine is uniform, but a considerable number of short wire-like nanoparticles are also obtained. The particle size of PtSn/C glycine is in the range from 3 nm to 12 nm with 7.2 nm of the average particle size. For PtSn/C PABA catalyst, severe aggregation is observed (as shown in Fig. 2d) and it is very difficult to measure its particle size. TEM results clearly show that the distribution and size of PtSn nanoparticles are strongly affected by the stabilizers. Our results are in good agreement with the results reported in the literature, e.g., the stabilizer can be used to control the morphology and size of the synthesized PtSn particle [16,17]. It is expected that the formed PtSn nanoparticles with different morphology and particle sizes would lead to the different electrocatalytic activity.

The electrochemical properties of PtSn/C catalysts were first examined by cyclic voltammetry (CV), which were carried out at 50 mV s^{-1} in N_2 saturated 1.0 mol L^{-1} H_2SO_4, in the potential range of −0.2 to 1.0 V *vs.* Ag/AgCl (Fig. 3). The characteristic features of Pt-based catalyst are observed for all PtSn/C catalysts, i.e., hydrogen adsorption/desorption peaks in the low potential region, oxide formation/stripping wave/peak in the high potential region, and a flat double layer in between [22]. At the same time, the differences in the total charges involved in the current–potential curves are apparent.

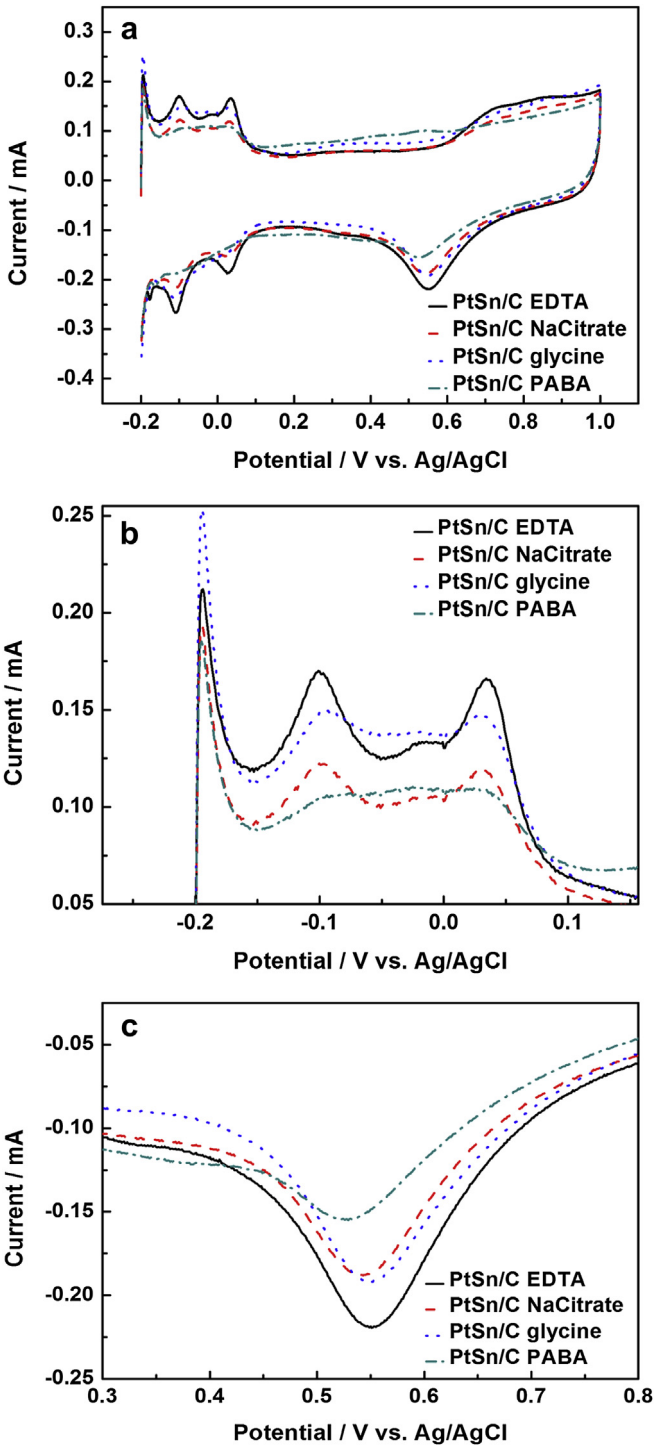

Fig. 3. (a) CVs of the PtSn/C catalysts in 1.0 mol L^{-1} H_2SO_4 at 50 mV s^{-1}. (b) The enlarged hydrogen desorption region. (c) The enlarged oxide reduction peaks.

The superficial states of synthesized PtSn/C catalysts can be qualitatively evaluated by analysis of the hydrogen adsorption/

Table 2
Electrochemical characterization of the four catalysts.

Catalyst	$ECSA_H$ ($m^2\ g^{-1}_{Pt}$)	$ECSA_{CO}$ ($m^2\ g^{-1}_{Pt}$)
PtSn/C EDTA	29.5	24.2
PtSn/C NaCitrate	20.7	16.3
PtSn/C glycine	28.2	23.4
PtSn/C PABA	14.5	19.6

desorption region, which was enlarged and shown in Fig. 3b. The hydrogen adsorption/desorption occurred on the surfaces of PtSn/C EDTA, PtSn/C NaCitrate, and PtSn/C glycine catalysts shows the typical features of polycrystalline Pt, which could result from Pt enrichment on the surface of PtSn nanoparticles. However, the CV of PtSn/C PABA catalyst shows the characteristic features of PtSn alloy, i.e., a vague hydrogen adsorption/desorption, which could be ascribed to a low metallic Pt content on the surface of PtSn/C PABA since Pt was alloyed with Sn.

In addition, the oxide reduction peak was chosen to measure the formation/reduction of oxide species on the electrocatalysts. Fig. 3c shows the enlarged oxide reduction peaks. The potential values of oxide reduction peaks reduce in the order: PtSn/C EDTA ≈ PtSn/C glycine > PtSn/C NaCitrate > PtSn/C PABA. It was reported that the high potential values is favorable to the desorption of the oxygenated adsorbates (e.g., OH_{ads}) formed on the surface of PtSn nanoparticles [23,24].

The electrochemical surface area (ECSA) of the metal particles provides important information regarding the number of electrochemically active sites on which the electrocatalytic reactions occur. From the monolayer adsorption of hydrogen on the Pt surface, ECSA values can be calculated by integrating the areas of hydrogen-adsorbed regions according to the Equation (4) [25]

$$ECSA_H = \frac{Q_H}{210 W_{Pt}} \quad (4)$$

where Q_H (C m^{-2}) is the average integrated charge in the hydrogen adsorption peak area in the CV curves after subtracting the charge from the double-layer region, W_{Pt} (g m^{-2}) is the Pt loading on the electrode, and 210 is the charge (mC m^{-2}) required to oxidize a monolayer of hydrogen on the Pt surface. The evaluated ECSA values are listed in Table 2, and found to follow the order PtSn/C EDTA > PtSn/C glycine > PtSn/C NaCitrate > PtSn/C PABA. The ECSA values are related to the distribution of PtSn nanoparticles on carbon support, which corresponds with the TEM results (Fig. 2).

Electrocatalytic activities of these PtSn/C catalysts for ethanol electrooxidation were measured by CVs in 1.0 mol L^{-1} C_2H_5OH + 0.5 mol L^{-1} H_2SO_4 solution with a scan rate of 50 mV s^{-1} at room temperature (Fig. 4). Since electrooxidation of ethanol at potentials below 0.3 V is largely blocked by adsorbed poisoning CO [9], ethanol oxidation occurs at potentials greater than 0.4 V (Fig. 4), where intermediates can be removed, and reaches the peak at about 0.7 V. From the practical point of view, the activation controlled region (around 0.2–0.3 V *vs.* Ag/AgCl) is important for the evaluation of catalyst activity. The inset in Fig. 4 is the enlarged region for the all catalysts. The current density increases in the order: PtSn/C PABA < PtSn/C NaCitrate < PtSn/C glycine < PtSn/C EDTA. The forward anodic peak current density of ethanol oxidation follows the following order: PtSn/C glycine > PtSn/C EDTA > PtSn/C NaCitrate > PtSn/C PABA. For all PtSn/C catalysts, the onset potentials of ethanol oxidation are almost the same, ca. 67 mV *vs.* Ag/AgCl. Fig. 5 shows the current–time curves recorded at 0.5 V, and the activities of four catalysts at 900th second are shown as the inset, which in general terms exhibit the same tendency observed in the CV study. Based on the above results, it can be concluded that the activities of these catalyst follow the order: PtSn/C glycine > PtSn/C EDTA > PtSn/C NaCitrate > PtSn/C PABA.

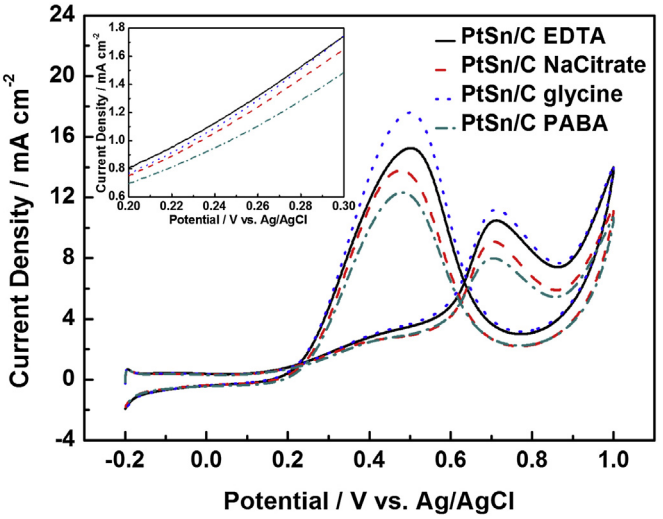

Fig. 4. CV curves obtained at 50 mV s^{-1} in H_2SO_4 1.0 mol L^{-1} + ethanol 0.5 mol L^{-1} for the all PtSn/C catalysts.

Fig. 6 shows the CO stripping voltammetry of these PtSn/C catalysts, where CO was pre-adsorbed in a 1.0 mol L^{-1} H_2SO_4 solution for 5 min. It can be seen that the adsorbed CO has been oxidized completely in the first scan, and no CO oxidation is monitored during the second scan for all catalysts. There are two main peaks, a low (marked with arrows) and a high potential peaks, in the all curves. Cherstiouk et al. [26] and Maillard et al. [27] found splitting of CO stripping peak for Pt nanoparticles synthesized by the wet chemical method and ascribed it to formation of nanograined Pt agglomerates. In line with the reports, the multiple CO stripping peaks observed on these PtSn/C catalysts were resulted from the agglomerates of PtSn nanoparticles. At the same time, Friedrich et al. [28] and Maillard et al. [27] reported the negative shift of CO oxidation was occurred due to the agglomeration of the nanoparticles. Here, the onset potential of the all catalysts are plotted and shown in Fig. 7. It can be seen that the onset negative shift increases with the degree of agglomeration.

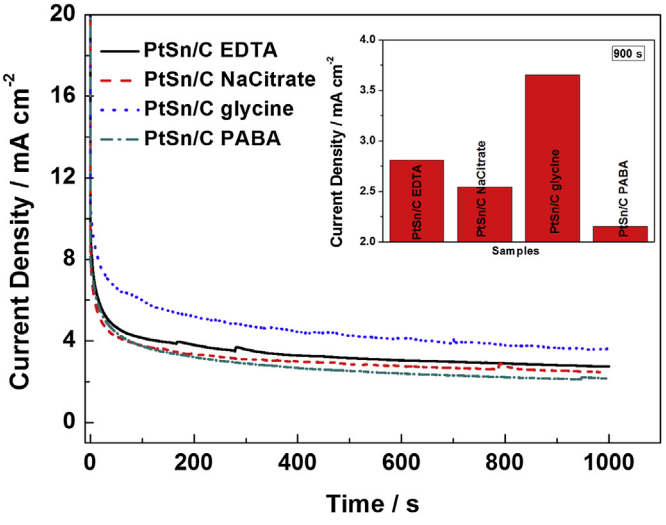

Fig. 5. Current density–time curves for ethanol oxidation obtained at 0.5 V of scan rate for the PtSn/C catalysts. Inset: current densities measured at 900 s. Electrolyte: 1.0 mol L^{-1} ethanol + 0.5 mol L^{-1} H_2SO_4.

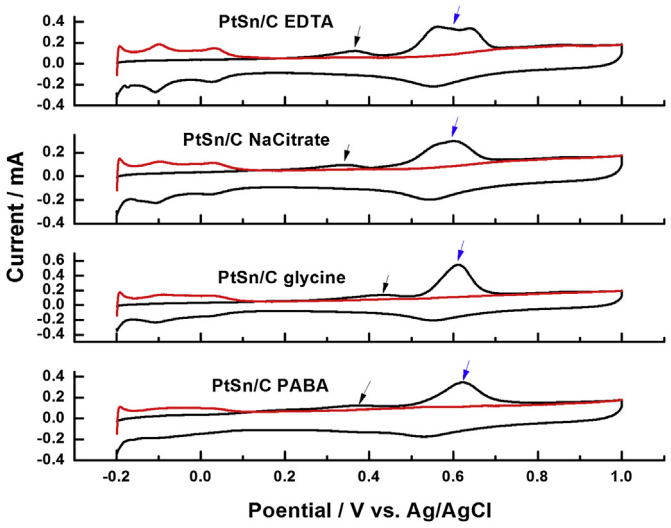

Fig. 6. CO stripping voltammograms of the PtSn/C catalysts in 0.5 mol L^{-1} H_2SO_4 solution at 50 mV s^{-1} of scan rate.

In addition, the active surface area of the catalysts for CO oxidation is another indicator of the electrocatalytic activity. The $ECSA_{CO}$ was calculated using the Equation (5) [29,30]

$$ECSA_{CO} = \frac{Q_{CO}}{480 W_{Pt}} \quad (5)$$

where $ECSA_{CO}$ is the electrochemical active surface area, Q_{CO} is the charge for CO desorption electro-oxidation in microcoulomb (μC), 480 is the charge required to oxidize a monolayer of CO on the catalyst and W_{Pt} is the metal loading. The calculated values of $ECSA_{CO}$ are listed in Table 2. The values of $ECSA_{CO}$ follow the order: PtSn/C EDTA > PtSn/C glycine > PtSn/C PABA > PtSn/C NaCitrate.

It is well-known that the activity of catalysts depends on several parameters, such as bulk and surface composition, alloying degree, particle size distribution and morphology. These factors can be controlled to enhance the activity of the catalysts by optimizing the synthesis parameters. In terms of bulk composition, it has been proven that PtSn/C catalyst with 3:1 of Pt:Sn atom ratio of bulk composition has the highest catalytic activity for ethanol oxidation [4,10]. However, there are the contradictory conclusions on the impact of alloying degree on the electrocatalytic activity towards ethanol oxidation. For instance, it was reported that the enhancement of electrocatalytic activity towards ethanol oxidation was attributed to a highly alloyed PtSn formed on the support [11,12]; however, Zhu et al. [31] reported that the PtSn/C catalysts with low alloying degree has better electrocatalytic activity towards ethanol oxidation. In this work, the bulk compositions of these four PtSn/C catalysts are 3:1 (Pt:Sn atom ratio), while the alloying degrees of four PtSn/C catalysts are slightly different. It wasn't found the direct relationship between the alloying degree and the electrocatalytic activity. Therefore, alloy degree of PtSn nanoparticles is not the factor that leads to the difference of electrocatalytic activity in our work.

In the process of the formation of PtSn nanoparticles, the reaction between the metal precursors is the primary step. At the same time, a competitive reaction to form metal complexes between metal ions and the stabilizers is occurring simultaneously. The rates of these two reactions affect the formation of particle nucleation and growth of nanoparticles as well as the composition of the alloy nanoparticles [16]. Therefore, even if the procedures of synthesizing nanoparticles are the same, the different stabilizers can lead to

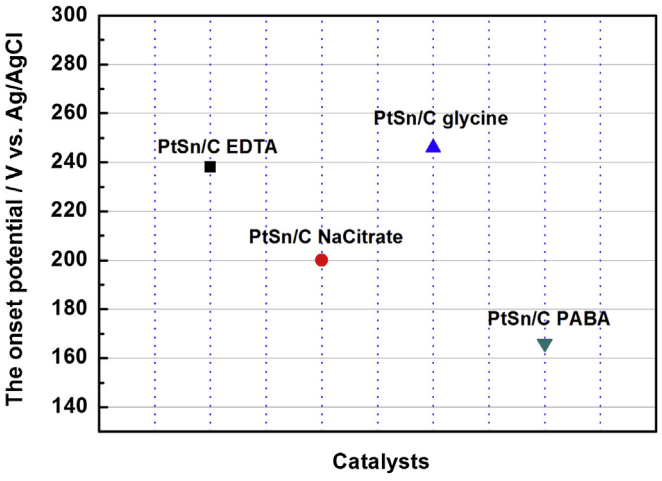

Fig. 7. The onset potential for CO oxidation of the PtSn/C catalysts derived from Fig. 6.

the different morphology and particle size distribution [16–18,32], and further result in the different electrocatalytic activities.

Based on the above results and discussion, we firstly divided the four catalysts into two categories in terms of the dispersion: i) PtSn/C EDTA and PtSn/C glycine, with good dispersion; ii) PtSn/C NaCitrate and PtSn/C PABA, with the severe agglomeration. The dispersion of PtSn/C EDTA and glycine is much better than that of PtSn/C NaCitrate and PABA, resulting in the larger electrochemical surface area, $ECSA_H$ and $ECSA_{CO}$, and higher electrocatalytic activities.

Although both PtSn/C EDTA and PtSn/C glycine have good particle dispersion, the PtSn/C glycine is more electrocatalytically active than PtSn/C EDTA. There two factors, i.e., surface composition and structure, which may be result in the difference of electrocatalytic activity between PtSn/C EDTA and PtSn/C glycine. XPS was carried out to investigate the surface composition and electronic structure of PtSn/C EDTA and PtSn glycine. Fig. 8 shows XPS survey spectra of the PtSn/C EDTA and PtSn glycine catalysts. The relative atomic ratios of Pt and Sn determined from the peak area are 7.7:1 and 5.8:1 for PtSn/C EDTA and PtSn glycine, respectively. It can be seen that the Pt content on the surface is obviously larger than the bulk, indicating that the Pt is enriched on the surface of PtSn nanoparticles. Besides, it can be seen that the Pt:Sn atomic ratio of

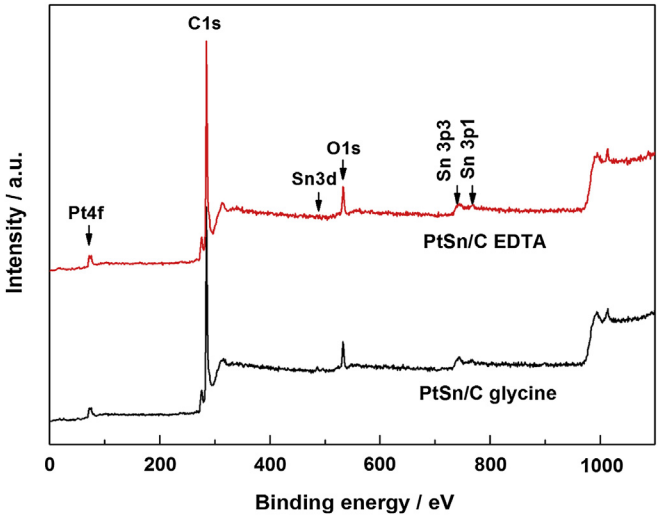

Fig. 8. XPS survey spectra of the PtSn/C EDTA and PtSn/C glycine catalysts.

PtSn/C EDTA is higher than that of PtSn/C glycine. Similar phenomenon was also reported [13].

Fig. 9 shows the Pt 4f photoelectron spectra of the PtSn/C EDTA and PtSn/C glycine catalysts. There are a high energy band (Pt $4f_{5/2}$) and a low energy band (Pt $4f_{7/2}$) at 75.2 and 71.7 eV, respectively. For two catalysts, both the shape and the position of Pt 4f are almost identical. Compared to Pt binding energies of Pt/C (74.4 eV, 71.3 eV) [20], it was found that Pt binding energies for both catalysts shift positively. Based on the electronegativity series (Sn, 1.96; Pt, 2.28), the addition of Sn in PtSn system means that charge transfer occurs from Sn to Pt which results in the lowering of Pt binding energy, i.e., the negative shift of Pt 4f binding energy. Villullas et al. found that the interaction between Pt nanoparticles and the RuO_2 particles leads to the positive shift of the Pt 4f binding energy [33]. It was also reported by other groups that the interaction between noble metal (Pt and Pd) and oxides leading to the positive shift of binding energies [34,35]. Hence, it could be presumed that the positive shifts of both PtSn/C catalysts result from the interaction between Pt and tin oxide species which can be further proved by the following Sn 3d XPS analysis.

To identify different chemical states of Pt on the surface of the PtSn/C EDTA and PtSn/C glycine catalysts, the Pt 4f spectrum was deconvoluted into three doublets which correspond to Pt $4f_{7/2}$ and Pt $4f_{5/2}$ of different oxidation states. The Pt $4f_{7/2}$ and Sn $3d_{5/2}$ binding energy and atomic percentage of PtSn/C EDTA and PtSn/C glycine are tabulated in Table 3. Chemical states and atomic percentage of Pt and Sn on PtSn/C EDTA and PtSn/C glycine are almost the same, implying that the difference of electrocatalytic activity isn't related to the chemical states of Pt.

Fig. 10 shows the Sn 3d XPS spectra of PtSn/C EDAT (a) and PtSn/C glycine. The Sn 3d spectra were deconvoluted into two components which are ascribed to elemental Sn and Sn oxides (e.g., SnO, SnO_2 or Sn hydroxides) [36]. To identify Sn(II) and Sn(IV) species from the XPS results is difficult due to the similar bonding energies [37,38]. The binding energies and relative intensities of elemental Sn and Sn oxides obtained from their XPS spectra are listed in Table 3. Table 3 shows that most of Sn is in oxidized state for both catalysts. The amount of Sn oxides in PtSn/C glycine is higher than that of PtSn/C EDTA. The Sn oxides could facilitate transfer of oxygen species for oxidation of adsorbed CO resulting from the dissociative adsorption of ethanol.

However, the effect of the content of Sn oxides on catalytic activity of PtSn-based electrocatalysts for ethanol oxidation is seldom studied. Moreover, the obtained result are not consistent. Liu et al. reported that Pt–SnO_x/C with 2.2 of Pt/Sn atomic ratio has better activity for ethanol oxidation than other atomic ratios [13]. The result obtained by Jiang et al. showed that Pt_3Sn/C with high content of Sn oxides, which was prepared by heat-treatment in Ar atmosphere, exhibited higher current than Pt_3Sn/C with lower content of Sn oxides, which was prepared by heat-treatment in O_2 atmosphere; but the open circuit potential of the former is positive compared to the latter [14]. In the work of Behm's group, a volcano curve can be observed with varied Pt/Sn atomic ratio for Pt/SnO_x/C catalysts, and the optimal ratio is 7/3 of Pt/Sn atomic ratio at room temperature [39]. These above results are not consistent since other effect, for example alloying degree, also play a role for ethanol oxidation. Thus, it is not sure that the result of the effect of the different amount of Sn oxides between PtSn/C glycine and PtSn/C EDTA on electrocatalytic activities for ethanol oxidation.

Table 3
The Pt $4f_{7/2}$ and Sn $3d_{5/2}$ binding energy and atomic percentage of the PtSn/C EDTA and PtSn/C glycine catalysts.

Catalyst		PtSn/C EDTA		PtSn/C glycine	
Pt $4f_{7/2}$	Species	Binding energy/eV	Percentage/%	Binding energy/eV	Percentage/%
	Pt(0)	71.6	34.4	71.6	34.0
	Pt(II)	72.4	32.8	72.4	33.0
	Pt(IV)	73.8	32.8	74.0	33.0
Sn $3d_{5/2}$	Sn(0)	485.7	37.6	485.8	12.9
	Sn(II/IV)	486.9	62.4	487.1	87.1

To clarify the main factor caused different activity between PtSn/C glycine and PtSn/C EDTA on electrocatalytic activities for ethanol oxidation, then, the difference of the morphology is considered. From Fig. 2, it can be found that the amount of short wire-like PtSn nanoparticles on PtSn/C EDTA and glycine catalysts is different. Similar short wire-like nanoparticles were also reported by Somodi et al. and Wang et al. [16,17]. They found that the wire-like nanoparticles were formed due to aggregation of quasi-spherical PtSn nanoparticles in one dimension. HRTEM was performed (Fig. 11) to investigate the structure of these wire-like nanoparticles formed on PtSn/C glycine. As shown in Fig. 11a, the short wire-like PtSn nanoparticles were formed *via* the aggregation of quasi-spherical PtSn nanoparticles. Isolated nanowire in Fig. 11b shows complex structures containing small crystallite interconnected *via* grain boundaries, implying the short wire-like PtSn nanoparticles are "nanostructured" material [40].

Nanostructured electrocatalysts [27,41] can enhance electrocatalytic activities due to the high density of inter-grain boundary regions in the nanoparticles. Here, since the wire-like nanoparticles were aggregated by quasi-spherical PtSn nanoparticles and the amount of short wire-like nanoparticles formed on PtSn/C glycine is greater than PtSn/C EDTA, the density of inter-grain boundary regions on PtSn/C glycine should be higher than that of PtSn/C EDTA. Thus, higher density of inter-grain boundary regions on PtSn/

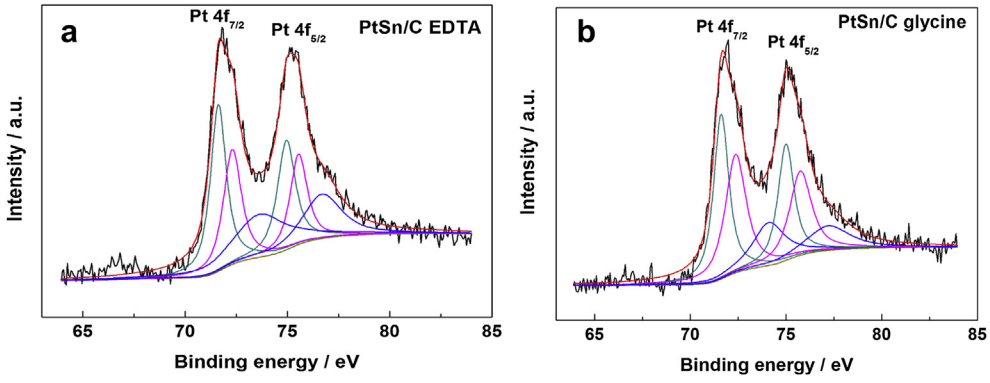

Fig. 9. The Pt 4f XPS spectra of the PtSn/C EDTA (a) and PtSn/C glycine (b) catalysts.

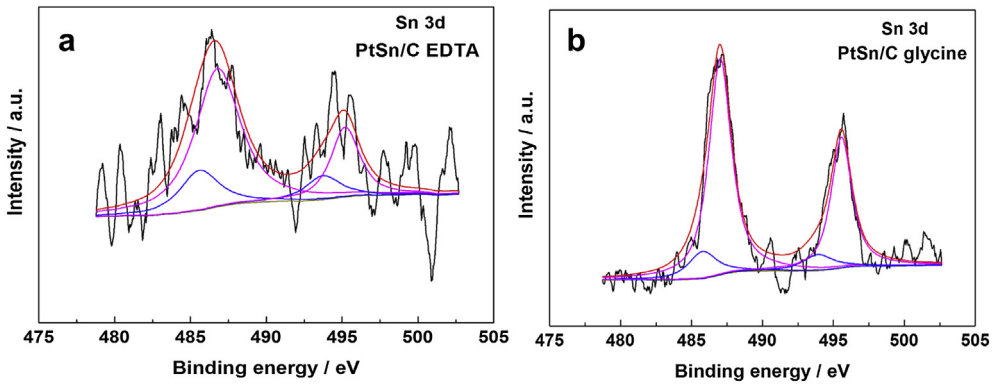

Fig. 10. The Sn 3d XPS spectra of the PtSn/C EDTA (a) and PtSn/C glycine (b) catalysts.

C glycine results in better electrocatalytic activity toward ethanol oxidation than PtSn/C EDTA.

4. Conclusions

Different stabilizers used to prepare PtSn/C catalyst can result in different PtSn nanoparticles formed on the carbon support. Stabilizers have a significant impact on the morphology and particle distribution of synthesized PtSn nanoparticles. The electrocatalytic activities towards ethanol oxidation of four PtSn/C catalysts increase in the order: PtSn/C PABA < PtSn/C NaCitrate < PtSn/C EDTA < PtSn/C glycine. Enhancement of electrocatalytic activity is ascribed to the high particle distribution of PtSn nanoparticles on the carbon supports. Furthermore, high density of inter-grain boundary regions existed on PtSn nanoparticles play a critical role in improving the electrocatalytic activity. The results showed that the electrocatalytic activity can be enhanced by choosing the appropriate stabilizer.

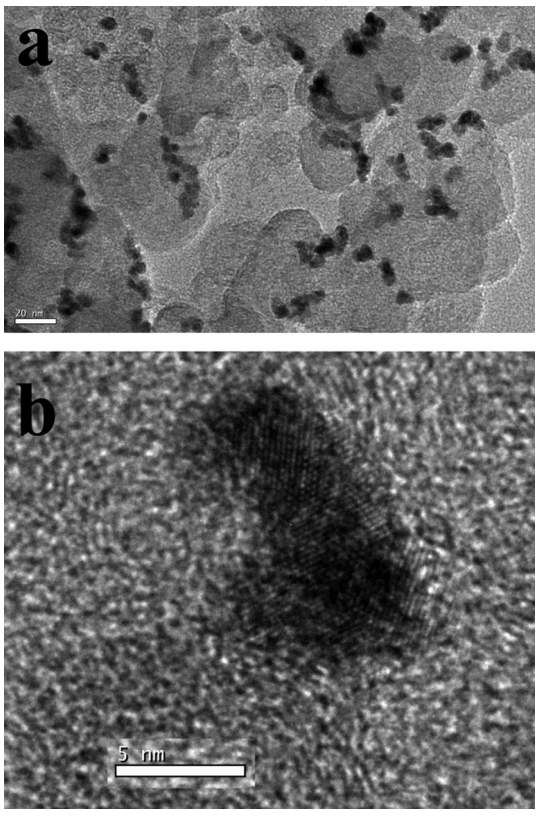

Fig. 11. TEM (a) and HRTEM (b) images of the PtSn/C glycine catalyst.

Acknowledgements

The authors would like to thank the National Natural Science Foundation of China (21163018, 21363022, and 51362027) for financially supporting this work.

References

[1] E. Antolini, E.R. Gonzalez, Catal. Today 160 (2011) 28.
[2] S. García-Rodríguez, M.A. Peña, J.L.G. Fierro, S. Rojas, J. Power Sources 195 (2010) 5564.
[3] C. Lamy, S. Rousseau, E.M. Belgsir, C. Coutanceau, J.M. Léger, Electrochim. Acta 49 (2004) 3901.
[4] L. Li, M. Huang, J. Liu, Y. Guo, J. Power Sources 196 (2011) 1090.
[5] K.L. Wang, H. Wang, S. Pasupathi, V. Linkov, S. Ji, R.F. Wang, Electrochim. Acta 70 (2012) 394.
[6] S.S. Gupta, S. Singh, J. Datta, Mater. Chem. Phys. 116 (2009) 223.
[7] J. Melke, A. Schoekel, D. Dixon, C. Cremers, D.E. Ramaker, C. Roth, J. Phys. Chem. C 114 (2010) 5914.
[8] P. Bommersbach, M. Chaker, M. Mohamedi, D. Guay, J. Phys. Chem. C 112 (2008) 14672.
[9] F.L.S. Purgato, P. Olivi, J.M. Léger, A.R. de Andrade, G. Tremiliosi-Filho, E.R. Gonzalez, C. Lamy, K.B. Kokoh, J. Electroanal. Chem. 628 (2009) 81.
[10] R.F.B. De Souza, L.S. Parreira, D.C. Rascio, J.C.M. Silva, E. Teixeira-Neto, M.L. Calegaro, E.V. Spinace, A.O. Neto, M.C. Santos, J. Power Sources 195 (2010) 1589.
[11] D.R.M. Godoi, J. Perez, H.M. Villullas, J. Power Sources 195 (2010) 3394.
[12] S.C. Zignani, V. Baglio, J.J. Linares, G. Monforte, E.R. Gonzalez, A.S. Aricò, Electrochim. Acta 70 (2012) 255.
[13] Y.H. Liu, F. Wu, C. Wu, Fuel Cells 12 (2012) 415–419.
[14] L. Jiang, Z. Zhou, Wenzhen Li, W. Zhou, S. Song, H. Li, G. Sun, Q. Xin, Energy Fuels 18 (2004) 866.
[15] F. Colmati, E. Antolini, E.R. Gonzalez, Appl. Catal. B 73 (2007) 106.
[16] F. Somodi, Z. Peng, A.B. Getsoian, A.T. Bell, J. Phys. Chem. C 115 (2011) 19084.
[17] X. Wang, J. Stover, V. Zielasek, L. Altmann, K. Thiel, K. Al-Shamery, M. Baumer, H. Borchert, J. Parisi, J. Kolny-Olesiak, Langmuir 27 (2011) 11052.
[18] Z. Liu, D. Reed, G. Kwon, M. Shamsuzzoha, D.K. Nikles, J. Phys. Chem. C 111 (2007) 14223.
[19] H. Wang, H. Da, S. Ji, S. Liao, R. Wang, J. Electrochem. Soc. 160 (2013) H266.
[20] X. Zhang, H. Wang, J. Key, V. Linkov, S. Ji, X. Wang, Z. Lei, R. Wang, J. Electrochem. Soc. 159 (2012) B270.
[21] J.C.M. Silva, L.S. Parreira, R.F.B. De Souza, M.L. Calegaro, E.V. Spinacé, A.O. Neto, M.C. Santos, Appl. Catal. B 110 (2011) 141.
[22] R. Wang, J. Jia, H. Li, X. Li, H. Wang, Y. Chang, J. Kang, Z. Lei, Electrochim. Acta 56 (2011) 4526.
[23] Y. Chen, Z. Liang, F. Yang, Y. Liu, S. Chen, J. Phys. Chem. C 115 (2011) 24073.
[24] H. Wang, R. Wang, H. Li, Q. Wang, J. Kang, Z. Lei, Int. J. Hydrogen Energy 36 (2011) 839.
[25] H. Wang, X. Zhang, R. Wang, S. Ji, W. Wang, Q. Wang, Z. Lei, J. Power Sources 196 (2011) 8000.
[26] O.V. Cherstiouk, P.A. Simonov, E.R. Savinova, Electrochim. Acta 48 (2003) 3851.
[27] F. Maillard, S. Schreier, M. Hanzlik, E.R. Savinova, S. Weinkaufb, U. Stimminga, Phys. Chem. Chem. Phys. 7 (2005) 385.

[28] K.A. Friedrich, F. Henglein, U. Stimming, W. Unkauf, Electrochim. Acta 45 (2000) 3283.
[29] Y.J. Ma, H. Wang, S. Ji, B.G. Pollet, R.F. Wang, ECS Trans. 50 (2012) 1943.
[30] W. Wang, H. Wang, J. Key, V. Linkov, S. Ji, R. Wang, Ionics 19 (2013) 529.
[31] M. Zhu, G. Sun, Q. Xin, Electrochim. Acta 54 (2009) 1511.
[32] X. Wang, L. Altmann, J. Stöver, V. Zielasek, M. Bäumer, K. Al-Shamery, H. Borchert, J. Parisi, J. Kolny-Olesiak, Chem. Mater. 25 (2013) 1400.
[33] H.M. Villullas, F.I. Mattos-Costa, L.O.S. Bulhoes, J. Phys. Chem. B 108 (2004) 12898.
[34] W.-L. Qu, Z.-B. Wang, Z.-Z. Jiang, D.-M. Gu, G.-P. Yin, RSC Adv. 2 (2012) 344.
[35] R. Awasthi, R.N. Singh, Int. J. Hydrogen Energy 37 (2012) 2103.
[36] Z. Liu, B. Guo, L. Hong, T.H. Lim, Electrochem. Commun. 8 (2006) 83.
[37] D.-H. Lim, D.-H. Choi, W.-D. Lee, H.-I. Lee, Appl. Catal. B 89 (2009) 484.
[38] D. Wang, S. Lu, S.P. Jiang, Electrochim. Acta 55 (2010) 2964.
[39] L. Jiang, L. Colmenares, Z. Jusys, G.Q. Sun, R.J. Behm, Electrochim. Acta 53 (2007) 377.
[40] H. Gleiter, Acta Mater. 48 (2000) 1.
[41] A.N. Gavrilov, E.R. Savinova, P.A. Simonov, V.I. Zaikovskii, S.V. Cherepanova, G.A. Tsirlina, V.N. Parmon, Phys. Chem. Chem. Phys. 9 (2007) 5476.